[Soft Matter

ARTICLE TYPE

Cite this: DOI: 00.0000/xxxxxxxxxx

Supplemental Information for Probing the dynamics of turbid colloidal suspensions using Differential Dynamic Microscopy †

Reece Nixon-Luke,[a] Jochen Arlt,[b] Wilson C.K. Poon,[b] Gary Bryant,*[a] and Vincent A. Martinez*[b]

S1 Sample concentrations

Sample concentrations used for the experiments. The volume fractions of the densest samples (pure stock solutions) are calculated based on the weight fractions specified by the supplier.

Sample	SYS250 Vol (%)	SYS210 Vol (%)	SYS140 Vol (%)
1	10.05	10.03	9.11
2	6.36	6.37	5.82
3	4.02	4.04	3.71
4	2.55	2.57	2.37
5	1.61	1.63	1.51
6	1.00	1.03	1.00
7	0.61	0.66	0.61
8	0.37	0.42	0.37
9	0.23	0.26	0.23
10	0.14	0.17	0.14
11	0.085	0.11	0.085
12	0.052	0.068	0.052
13	0.032	0.043	0.032
14	0.019	0.027	0.019
15	0.012	0.017	0.012
16	0.0072	0.011	0.0072
17	0.0044	0.007	0.0044
18	0.0027	0.0044	0.0027
19	0.0016	0.0028	0.0016
20	0.001	0.0018	0.001

Table S1: Values of volume fraction ϕ used for preparing the solutions using SYS250, SYS210, and SYS140.

[a] *School of Science, RMIT University, Melbourne, Victoria 3000, Australia.*
[b] *b. SUPA, School of Physics & Astronomy, The University of Edinburgh, Peter Guthrie Tait Road, Edinburgh, EH9 3FD, United Kingdom.*
* corresponding authors E-mails: vincent.martinez@ed.ac.uk; gary.bryant@rmit.edu.au.

S2 Experimental procedure for DDM measurements

As briefly outlined in the main manuscript, we typically used movies which had the same mean intensity $\bar{I}$ (close to 128, the middle of the dynamic range of our 8 bit camera). This was in general achieved by adjusting illumination intensity and exposure time while observing a live intensity histogram. However, to enable us to perform a more quantitative comparison of transmission and DDM signal amplitudes across a wide range of sample volume fractions, we recorded several sets of movies for which we kept almost all experimental conditions fixed. In particular the illumination settings, sample thickness L and position z were kept the same. The only parameter that was adjusted was the camera exposure time, as the limited dynamic range of our camera was too small to deal with the large change of the transmitted light intensity. We used the following experimental protocol:

1. Focus the objective close to the middle of the sample (also see below).
2. Set up Köhler illumination. We reduced the numerical aperture of the illumination from 0.55 to ≈ 0.3 to enhance image contrast while ensuring a sufficiently bright illumination.
3. Start imaging the densest sample using the highest bright field illumination and adjust exposure time to achieve $\bar{I} \approx 128$. For some of these very dense samples the experimentally achievable $\bar{I}$ was somewhat lower even for the longest possible exposure time compatible with the frame rate.
4. Test progressively more dilute samples, reducing the camera exposure time to keep the mean intensity on the camera $\bar{I} \approx 128$.
5. Record a movie of a water sample (i.e. without any colloids) as a reference.

By keeping track of the exposure time Δt, we can scale the measured mean intensities using the proportionality $\bar{I} \propto \Delta t$ to calculate the transmission relative to the sample without colloids as shown in fig. 5 of the main manuscript. An overview of the main settings used for the various results presented in the manuscript are summarised in table S2.

Using a camera with a higher dynamic range, such movie sets could possibly be recorded without the need of changing any experimental settings at all.

Figure	Particle size (nm)	Capillary height L (μm)	image dimension (pixels)	Frame rate (fps)	number of frames	Illumination settings
3	250	400	1024	100	6000	adjusted
4	250, 140	400, 100	1024	100	6000	adjusted
5	210	400	512	100	10000	fixed
6	250	100, 200, 400	512	100	10000	fixed
7	210	400	512	100	10000	fixed
8	250	400	512	1000	20000	fixed
9	250	100, 200, 400	512	1000	20000	fixed
10	210	400	512	1000	20000	fixed

Table S2: Experimental conditions for each individual figure. For 'adjusted', the incident lamp power was altered and the camera exposure was kept constant. For 'fixed', the lamp power and all other illumination settings were kept constant and the only camera exposure was adjusted.

.

Focusing into very dense samples of sub-resolution colloidal suspensions is experimentally not trivial, especially on a manual microscope as used in this study. For the densest samples, the only reference points that could be reliably identified from the camera images were the lower and upper *outer surfaces* of the glass capillaries. For consistency we therefore always identified these 2 positions and then moved the microscope objective exactly halfway in between. Note that this is *not* exactly in the middle of the sample but somewhat closer to the objective, due to the fairly thick walls of the glass capillaries having a larger refractive index than our aqueous suspensions. For capillaries with height $L = 400\mu$m with glass wall thickness of 400μm this leads to $z = 130\mu$m. Similarly, for $L = 100\mu$m we have $z \approx 40\mu$m and for $L = 200\mu$m we have $z \approx 75\mu$m. The results showing the signal as a function of imaging depth z (fig. 7 in main manuscript) are corrected for the difference in refractive index and correspond to the geometrical position of the image plane relative to the bottom of the sample.

S3 DLS and TCDLS plots

Figure 3 of the manuscript shows typical DICFs measured from DDM. Here, in Fig. S1, we show typical intensity correlation functions measured with DLS and TCDLS.

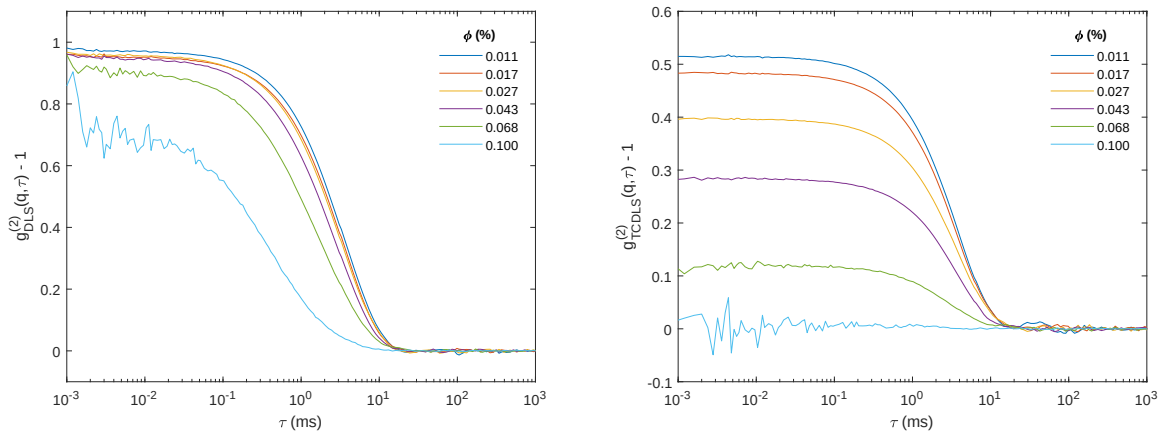

Fig. S1: g_{DLS} (left) and g_{TCDLS} (right) for SYS250 $\phi = 0.01$ to 0.1%. As ϕ increases, the DLS data shows a quicker decay rate, whereas the TCDLS data shows the same decay rate with a reduced intercept.

S4 Estimating the photon mean free path ℓ

In addition to the estimation of ℓ based on the measured mean intensity of the recorded movies detailed in the main manuscript, ℓ was also measured for SYS210 using a laser based setup as pictured in Fig. S2. The laser (Aerotech) was sent through a 10 mm quartz cuvette containing the sample, and the transmission I was measured using a power meter (Thorlabs S130C) for $\phi = 0.068\%$, 0.027%, 0.011%, 0.0044%, and 0.0017%. The transmission I_0 was measured using the cuvette filled with water. Three measurements were averaged for the final value of I. Fig. S3 shows I/I_0 vs ϕ from these measurements. This gives $\ell = 189\mu\text{m}\%/\phi$.

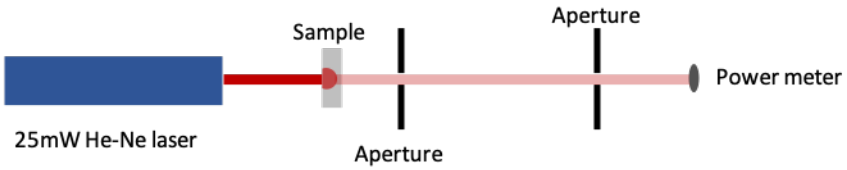

Fig. S2: Schematic of the laser-based setup to measure the photon mean free path ℓ of SYS210.

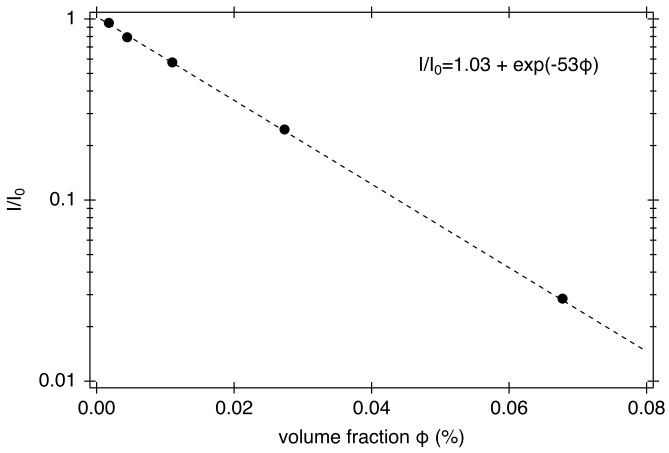

Fig. S3: Plot of I/I_0 vs ϕ for the calculation of the mean free path.

Our experimental data can also be compared to theoretical predictions based on Mie scattering theory for spherical scatterers. Online Mie Scattering calculators such as Scott Prahl's Mie Scattering Calculator (`https://omlc.org/calc/mie_calc.html`) make it straightforward to calculate scattering cross-sections and other scattering parameters. Using $d = 210\,\text{nm}$, $n_{\text{water}} = 1.332$, $n_{\text{PS}} = 1.586$ and a representative wavelength of $\lambda = 633\,\text{nm}$ gives $\sigma = 0.00297\,\mu\text{m}^2$ for the scattering cross-section. With $\ell = V_{\text{sc}}/(\sigma\phi)$, where $V_{\text{sc}} = 0.00485\,\mu\text{m}^3$ is the volume of a single scatterer, this leads to $\ell(\phi) = 163\,\mu\text{m}\%/\phi$, which we consider in very good agreement with our experimental measurement considering the uncertainties in the parameters involved in the calculation.

Link to the full calculations: `https://omlc.org/cgi-bin/mie_angles.cgi?diameter=.21&lambda_vac=0.633&n_medium=1.332&nr_sphere=1.586&ni_sphere=0&n_angles=100&density=1`.

S5 Estimating ϕ_s at which multiple scattering emerges

To further understand DDM for turbid samples, it is useful to identify the volume fraction ϕ_s, corresponding to the ϕ-boundary between single scattering regime and when multiple scattering emerges. In the main text, we estimated ϕ_s directly from the amplitude of the DDM signal $\langle A \rangle$ by identifying the volume fraction when $\langle A \rangle$ first deviates from linearity with ϕ. From DDM measurements performed at $L = 400\,\mu\text{m}$, we found $\phi_s(L = 400\,\mu\text{m}) \approx 0.1\%$ corresponding to $\ell \approx 1.6\text{mm}$, and thus $\ell/L \approx 4$. Here we show that this is consistent with a second approach based on TCDLS data.

From figure 4 of the manuscript, we defined the volume fraction at which multiple scattering emerges in the TCDLS data (using $L = 4\,\text{mm}$) by identifying the first value of ϕ where the TCDLS intercept first decreases. This gives $\phi_s(L = 4\,\text{mm}) = 0.058 \pm 0.14$ and 0.0155 ± 0.007 for SYS250 and SYS140, respectively. Using figure 5b of the manuscript, we estimated $\ell(\phi_s) = (20 \pm 5)\text{mm}$ and $(24 \pm 6)\text{mm}$ for SYS250 and SYS140, respectively. Note that the error bars represents standard deviation and is dominated by the large spacing in volume fraction values. We found $\ell/L \approx 5 - 6$, and thus expect multiple scattering to emerge for $L/\ell \geq 1/5$, where single scattering constitutes $\approx 90\%$ of the signal. This result is quantitatively consistent with our approach solely based on DDM measurements and presented in the section 4.2 of the manuscript.

S6 Further analysis on effect of imaging depth z

In Figure 7 of the main text, we show that the measured diffusion coefficient, D, decreases when z is decreased from $z = 50\,\mu\text{m}$. This decrease in D could potentially be due to hydrodynamic interactions between the particles and the wall. However, using a well-known approximation due to Faxén, we find that the diffusivity of a 210 nm diameter sphere at $z \approx 10\,\mu\text{m}$ away from a hard wall is reduced by $\lesssim 0.5\%$ from its bulk value, far too small to account for the observed $\sim 5\%$ decrease, which is not reached until $z/R \lesssim 10$, or $z \sim 1\,\mu\text{m}$. Closer inspection of the videos used to obtain the results presented in Figure 7 of the main text reveal the presence of a small number of clearly visible large diffusing particles. These particles, most likely aggregate clusters of our colloids, have sedimented to the bottom of the capillary, where they accumulate over time. We identified 2 subregions in the movies where bigger particles were observed (BR) or were absent (TL) at the bottom of the capillary ($z \approx 0\,\mu\text{m}$). Figure S4 shows that there is no decrease in D for the ROI free of the bigger sedimented particles, except for $z \approx 0\,\mu\text{m}$. This shows that the decrease in diffusivity shown in the figure 7 is mainly due to the presence of sedimented particles.

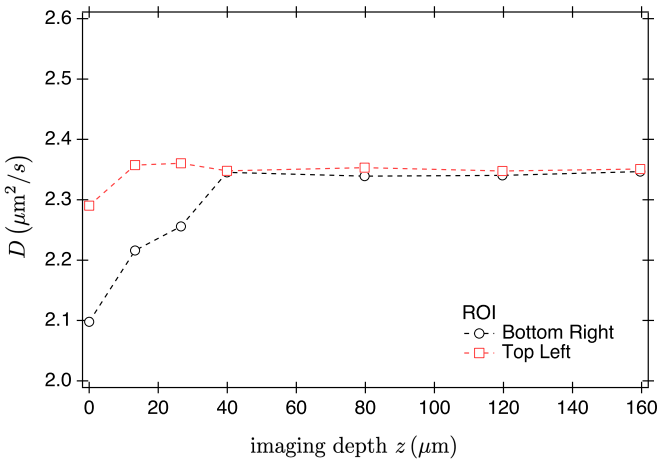

Fig. S4: DDM analysis of the movies recorded for Figure 7 of the main text but applying a region of interest for which big sedimented particles were either observed (BR) or not (TL).

S7 Experimental estimation of depth of field

To experimentally evaluate the depth of field we follow the experimental protocol recently demonstrated by Aime *et al.*[1]. We acquired a z-stack through a static sample using two extremes values of the illumination numerical aperture (0.52 and 0.025), which were then analysed using the standard DDM protocol. But now the independent variable is the difference in z-position. We use $\Delta z_{1/2}$ where the resulting DICF has increased to half of its plateau value as an estimate for the depth of field DoF$= 2\Delta z_{1/2}$. Fig. S5 shows the resulting DoF as a function of q. At small q values the depth of field becomes large, especially if the numerical aperture of the illumination is kept low (see fig. S5). Note that the experimental data presented in the manuscript was acquired with an illumination numerical aperture of 0.3, i.e. close to the full illumination NA shown in fig. S5.

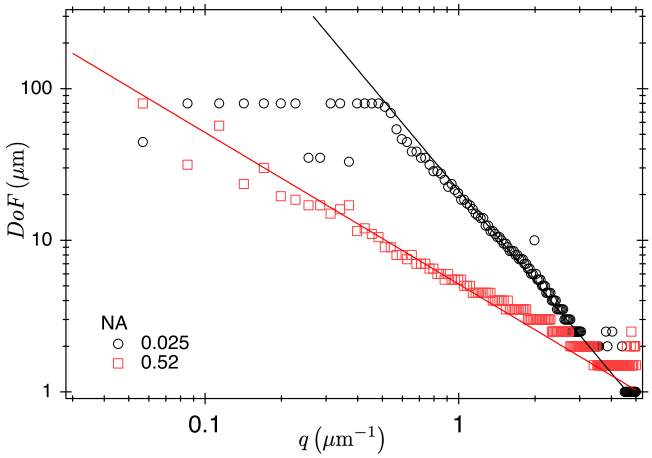

Fig. S5: Experimental estimates for the depth of field for a 60× objective when using either the full NA of the condenser (0.52) or a small diameter of the aperture diaphragm, reducing the illumination NA to ≈ 0.025. Note that the apparent saturation at DoF $\approx 80\mu$m is an artefact due to the limited extent of our experimental stack.

S8 Emergence of a short-time process at low q

We show in Fig. S6 that the parameters associated with the short-time process are approximately independent of q. Note that noise increases for lower volume fractions, for which the contribution from multiple scattering are weak.

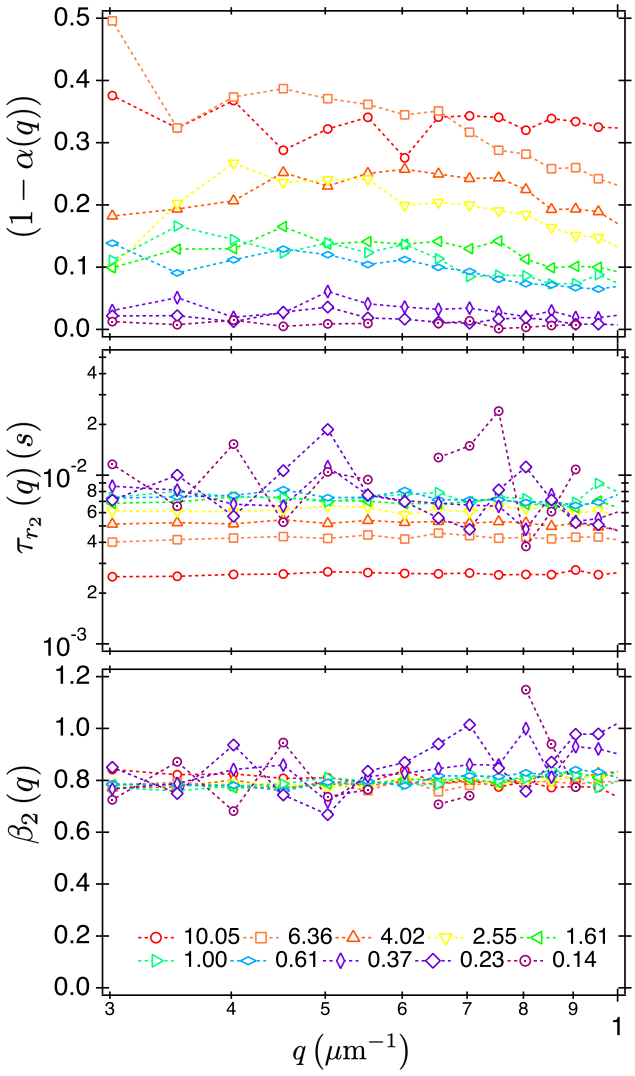

Fig. S6: Amplitude $(1-\alpha)$, timescale τ_{r_2}, and exponent β_2 as a function of q for $L = 100\mu$m for several volume fraction ϕ as indicated in legend.

In the discussion of the main text, we argue that the values of the measured depth of field, DoF, encompass well the range of values of the photon mean free path ℓ at higher volume fractions, so that at low values of q: DoF$\gtrsim \ell$ and at high values of q: DoF$\ll \ell$. Thus, we expect the observation of a short-time process, associated with multiple scattering, predominantly at low q first. Fig. S7 below shows that this is indeed the case.

Notes and references

1 S. Aime and L. Cipelletti, *Soft Matter*, 2019, **15**, 213–226.

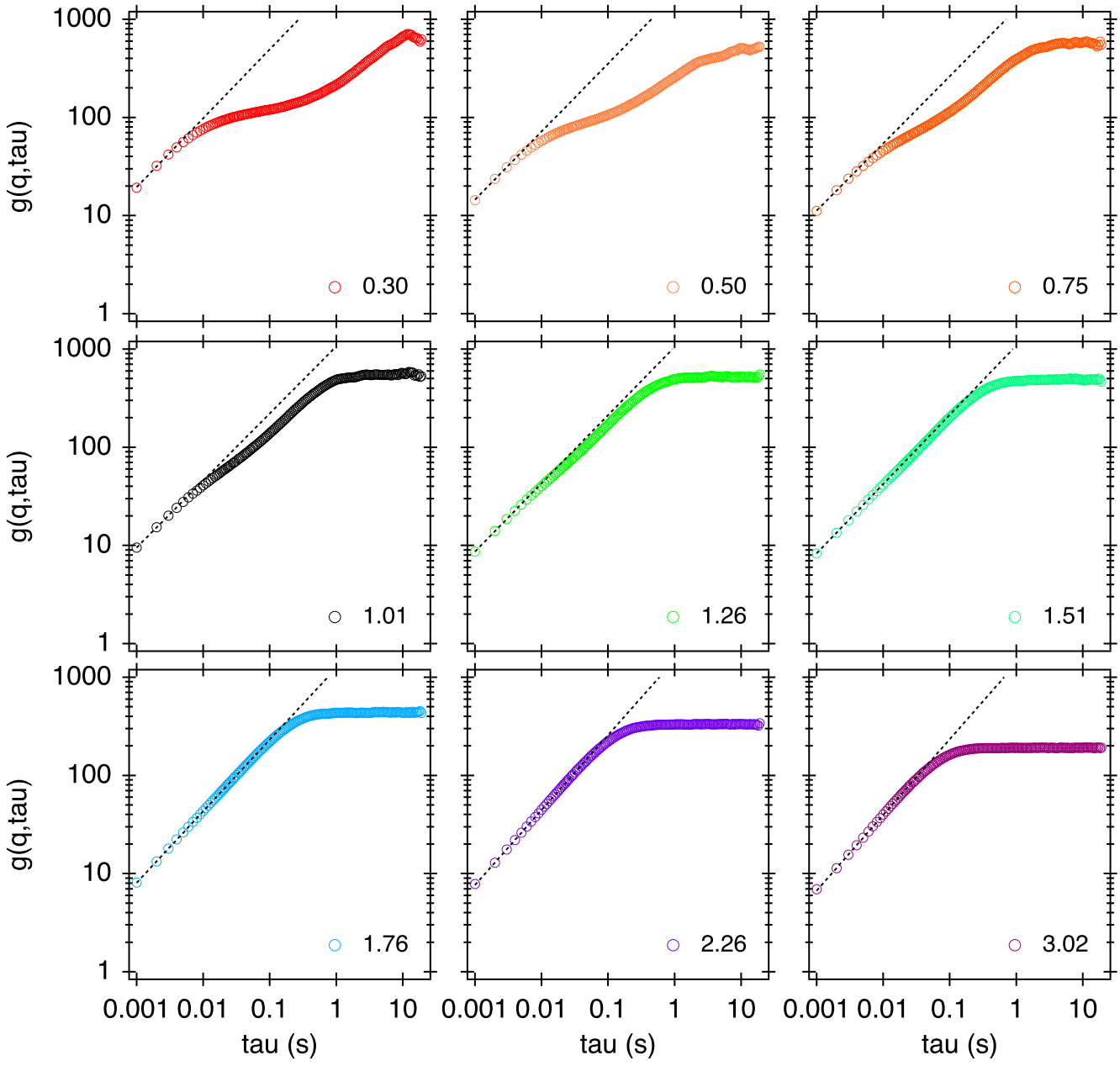

Fig. S7: DICFs of SYS250 at $\phi = 1.6\%$ for $L = 100\mu$m for several q values. An inflection point, i.e. signature of short-time process, is emerging at $q \approx 1.2\mu\text{m}^{-1}$ and observed through the emergence of deviation from a power law fit (dotted lines) performed at very short delay time $\tau \leq 0.01$ s.